Advances in Water Resources 33 (2010) 1320–1330

Contents lists available at ScienceDirect

Advances in Water Resources

journal homepage: www.elsevier.com/ locate/advwatres

Characterizing hyporheic transport processes — Interpretation of electrical geophysical data in coupled stream–hyporheic zone systems during solute tracer studies

Adam S. Ward [a,*], Michael N. Gooseff [a], Kamini Singha [b]

[a] Department of Civil and Environmental Engineering, The Pennsylvania State University, 212 Sackett Building, University Park, PA 16802, USA
[b] Department of Geosciences, The Pennsylvania State University, University Park, PA 16802, USA

ARTICLE INFO

Article history:
Received 19 November 2009
Received in revised form 14 May 2010
Accepted 29 May 2010
Available online 8 June 2010

Keywords:
Hyporheic
Hydrogeophysics
Electrical resistivity
Stream solute

ABSTRACT

Quantifying hyporheic solute dynamics has been limited by our ability to assess the magnitude and extent of stream interactions with multiple domains: mobile subsurface storage (MSS, e.g., freely flowing pore water) and immobile subsurface storage (ISS, e.g., poorly connected pore water). Stream-tracer experiments coupled with solute transport modeling are frequently used to characterize lumped MSS and ISS dynamics, but are limited by the ability to sample only "mobile" water and by window of detection issues. Here, we couple simulations of near-surface electrical resistivity (ER) methods with conservative solute transport to directly compare solute transport with ER interpretations, and to determine the ability of ER to predict spatial and temporal trends of solute distribution and transport in stream–hyporheic systems. Results show that temporal moments from both ER and solute transport data are well correlated for locations where advection is not the dominant solute transport process. Mean arrival time and variance are especially well-predicted by ER interpretation, providing the potential to estimate rate-limited mass transport (i.e. diffusive) parameters from these data in a distributed domain, substantially increasing our knowledge of the fate and transport of subsurface solutes.

1. Introduction

The movement of stream water into relatively slow-moving domains increases reach residence time of water and solutes [1,2]. By slowing the movement of water within a reach, the potential for processing of nutrients and other solutes is increased through longer exposure of stream solutes to microbial communities and biogeochemically active sediment [3–5]. Understanding the transport and fate of stream solutes is critical to understanding the temporal and spatial distribution of biogeochemical cycling associated with hyporheic exchange in streams.

Stream solute transport studies frequently yield concentration time series from in-stream and subsurface monitoring locations with long tails that are not explained by the in-stream processes of advection and dispersion alone. The movement of solute from the highly advective mobile domains into less-mobile domains with heterogeneous residence times is a common explanation of the observed tailing behavior in hydrological sciences. This type of tailing behavior has been observed in both flow through porous media [e.g., 6,7] and the exchange of stream water with the less-mobile hyporheic zone [e.g., 8,9]. Movement of tracer into the slower moving in-stream dead zones and into the hyporheic zone is typically considered responsible for this tailing behavior in stream–hyporheic studies. However, most stream solute studies overlook the range of mobile domains in the hyporheic zone, where domains range from highly advective and mobile (i.e., free pore water) to immobile (i.e., dead-end pore space, bound pore fluid) [10].

Tracer studies are frequently used to estimate interaction between mobile and immobile domains in both streams and porous media, yet there are inherent flaws in their formulation and interpretation. Stream-tracer studies rarely yield a full mass recovery, even with in-stream monitoring at substantial distances downstream, due to flux of labeled water into larger spatial and temporal scale flowpaths than can be observed with common tracer techniques [11,12]. The space and time scales that can be characterized in stream-tracer experiments are commonly referred to as a "window of detection" [13]. Payn et al. [12] investigated, among other characteristics, mass loss along a mountain headwater stream, finding mass loss of over 10% through a 200 m reach that was not explained by groundwater flow out of the system. They identified flowpaths providing tracer loss to deeper, slower moving flowpaths as one potential fate for tracer. Typical solute monitoring methods (i.e. wells), however, are insufficient to characterize these low-concentration, spatially complex flowpaths due to their sensitivity to a limited spatial scale, and because well samples only characterize the mobile subsurface (MSS) water in the

* Corresponding author. Tel.: +1 989 860 9252; fax: +1 814 863 7304.
E-mail address: asw178@psu.edu (A.S. Ward).

0309-1708/$ – see front matter © 2010 Elsevier Ltd. All rights reserved.
doi:10.1016/j.advwatres.2010.05.008

immediate vicinity of a monitoring well. Consequently, concentration breakthrough curves are largely indicative of the mobile domain; despite this fact, they are used to infer characteristics of less-mobile domains, including exchange rates and physical characteristics [14]. Because field observations of mobile domain concentration alone are used to quantify unobserved domains, the results are often not physically meaningful [15,16]. In stream–hyporheic studies, installation of invasive monitoring well networks provides discrete point observations that provide only discrete, point assessment of the temporal or spatial distribution of tracer within the subsurface. Additionally, the stream-tracer approach is limited by a window of detection that is commonly focused on hyporheic flowpaths occurring at short temporal (e.g., seconds to hours) and spatial (millimeters to tens of meters) scales [13]. The relative scales of advection vs. diffusive processes (including transfer between mobile and less-mobile domains known as rate-limited mass transfer (RLMT)) suggest that stream-tracer studies considering only data in-stream, or in shallow monitoring wells, are biased toward short spatial and temporal flowpaths [17], despite a recognition that exchange occurs on larger scales. Indeed, Harvey et al. [18] found that common transient storage modeling techniques [9] provided a good fit for short, rapid exchange with gravel bar sediment, but a poor fit for solute transport within slower MSS flowpaths.

Despite the recognition of a bicontinuum of MSS and immobile subsurface (ISS) zones, stream transport modeling has often lumped all immobile domains into one set of physical and chemical coefficients. Only recently has stream solute transport modeling begun to address multiple scales of storage [e.g., surface vs. hyporheic transient storage, 19], and no models have yet addressed solute transport processes in the hyporheic-bicontinuum, i.e. simulation of both MSS and ISS. To calibrate more complex model formulations, additional field observations are required. In the past, multiple storage-zone models have relied on observations in monitoring wells and direct sampling from in-stream dead zones to provide the additional data required. A spatially distributed characterization of hyporheic solute transport would require more monitoring wells than can feasibly be installed and monitored during a typical tracer study.

To overcome the data limitations used in solute transport monitoring and modeling, we explore the use of electrical resistivity (ER) measurements to quantify hyporheic solute transport processes. ER methods pass direct current (or low-frequency alternating current) through a soil–water matrix, and can be used to estimate the spatial and temporal distribution of electrical resistivity. ER has been used to track saline tracers across a range of scales, including changes in hyporheic salinity for a tidal creek [20], aquifer storage and recovery tests [21], and transport through porous media in both laboratory [22] and field-scale two- and three-dimensional experiments monitoring tracer (frequently saline) plumes [23–27]. Near streams, these data have been successfully used to generate tomograms, or maps of subsurface electrical conductivity, which highlight the spatial distribution of the stream tracer in the subsurface [28], and to investigate subsurface architecture [29]. Despite its demonstrated capabilities, ER is limited by our difficulty in defining the support volume of the measurement [30]. While ER data provides spatially integrated measurements over broad spatial areas with the potential to do so at a high temporal frequency, determining the depth of penetration or the volume averaged by a single measurement is difficult and dependent on the electrode geometry and electrical resistivity of the subsurface [31,32].

Numerical studies by Singha et al. [33] suggest the potential of ER for hyporheic assessment using conservative, electrically conductive tracers is great. The studies suggest that ER results are useful for calculation of solute transport parameters, including the immobile fractions of pore space, and the RLMT coefficient that controls the rate of exchange between the domains. Singha et al. [33] worked with inverted tomographic results, which are complicated by the assumptions inherent within inversion [34], and was limited by assumptions inherent in the solute transport model [OTIS, 35]. Limiting assumptions include a well-mixed storage zone with no downstream transport in the subsurface. Here, we seek to address these limitations by working with non-inverted electrical responses and utilizing a single, coupled model to simulate solute transport in three dimensions. This more complex model produces ER data more representative of field studies, and thus better enables interpretation of electrical response to assess the distribution of solute within multiple subsurface domains. Without an understanding of ER sensitivity to multiple processes, occurring in a dynamic system, we cannot reliably interpret field data. Our numerical solute transport model accounts for RLMT between MSS and ISS domains while advection and dispersion drive exchange of the solute between the stream and MSS domains. The model formulation allows us to explore the contributions of solute presence or absence in the highly mobile stream domain, in combination with both mobile and immobile domains within the hyporheic zone to aid in interpretation of ER data.

To the best of our knowledge, the interpretation of ER data (as opposed to tomograms) during a stream–hyporheic tracer study has not been attempted. Here, we focus on the potential to use temporal moment analysis to discern the dominant solute transport processes within a stream–hyporheic system. This study provides a framework for collection and interpretation of ER data during these studies, and demonstrates a novel application of ER. We expect that the presence of electrically conductive tracer in different domains (mobile and immobile) and distributed in the subsurface by spatially varied transport processes will exhibit differing responses in the ER data. The objectives of this study are to use a numerical model (1) to investigate the ability of an ER surface array to predict spatial trends and temporal moments of solute concentrations during a stream–hyporheic tracer study; and (2) to use ER and solute transport data to identify the distribution of dominant solute transport processes in the subsurface.

2. Numerical simulation

2.1. Numerical model formulation

We used COMSOL [36], a fully coupled finite-element model, to simulate solute transport within and between domains, in addition to simulation of ER measurements. Model geometry is based on an idealized 3rd order pool–riffle-step morphology [37], with a channel 2 m in width (Fig. 1). A series of geomorphologic pool–riffle-step sequences was modeled to drive hyporheic exchange within the model. ER measurements focused on the third riffle from the upstream boundary (Fig. 1) to avoid model boundary effects, and condition inflow and outflow in the area of interest. A floodplain on either side of the stream was modeled, extending 10 m from the stream surface. An active substrate depth of 5 m was included above a no-flow boundary. A stream flow rate of 0.17 m^3/s was simulated in the channel. Groundwater flow was modeled with fixed head at the upstream and downstream model extents corresponding to the elevation of the stream surface. Hydraulic conductivity in the entire subsurface was assigned as homogeneous and isotropic, at 1.0×10^{-3} m/s. The model domain was bounded by no-flux conditions on the top, bottom, and lateral extents, such that all flow entered the upstream and exited the downstream ends of the domain with no lateral inflow or outflow. No unsaturated zone was included in the model domain. A total of 123,808 finite elements were simulated in the model domain with average element to volume ratios of 2.50×10^{-4} for the flow and solute transport domains (regions "Subsurface" and "Stream" in Fig. 1B) and 1.68×10^{-5} for the outer domain added to minimize edge effects for the ER model (region "ER Only" in Fig. 1B).

Solute transport in the stream and MSS domains is simulated by the advection–dispersion equation. Stream flow was modeled as well-mixed in the vertical and transverse dimensions by assigning a dispersivity of 1 m in these directions, yielding essentially one-dimensional flow with no

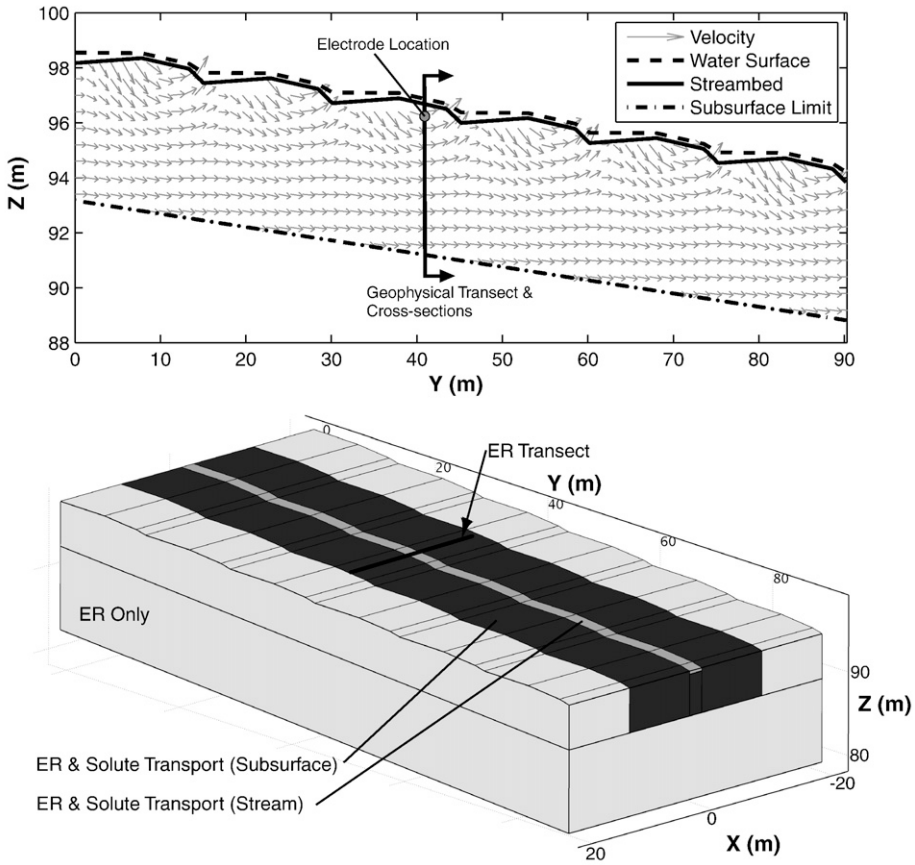

Fig. 1. (A) Profile of model showing steady-state velocity in the subsurface. Model results yield similar velocity profiles to two-dimensional results published by Gooseff and others [37]. A no-flow boundary is enforced at the subsurface limit, with velocity parallel to the bed as shown by the bottom arrow in each column. (B) Isometric view of model geometry. Profile view to show pool–riffle-step geomorphology and highlight the velocity patterns observed in the subsurface.

in-stream transient storage. Longitudinal dispersion in the channel was set at 3.45×10^{-7} m^2/s. In the subsurface, an immobile domain was partitioned from the mobile porosity as 50% of the 35% total porosity, and assigned a diffusion coefficient of 1.0×10^{-4} m^2/s. Parameters were selected to be representative of a headwater mountain stream with a subsurface of mixed gravel, sand, and silt. In addition to the advection-dispersion equation, first-order RLMT was parameterized using the following equations for exchange in the solute transport advection–dispersion equation.

$$\frac{\partial C_{MSS}}{\partial t} = \alpha(C_{ISS}-C_{MSS}) \quad (1)$$

$$\frac{\partial C_{ISS}}{\partial t} = -\alpha\frac{\theta_{MSS}}{\theta_{ISS}}(C_{ISS}-C_{MSS}) \quad (2)$$

where C_{MSS} and C_{ISS} are the MSS and ISS concentrations [kg/m^3], α is the exchange coefficient [d^{-1}], and θ_{MSS} and θ_{ISS} the MSS and ISS porosities [unitless]. The exchange coefficient was set as $\alpha=1.0\times10^{-3}$ d^{-1} (within the range of values from [33]). For this study, we conceptualize the subsurface as consisting of both mobile and immobile space, with a single coefficient describing RLMT. In field settings, heterogeneity and scale effects of the exchange coefficient should be considered. Despite this simplification, these models provide insight into hyporheic transport processes that are overlooked by many stream-tracer studies.

2.2. Simulated tracer injection

To assess the sensitivity of electrical geophysics to the presence of the electrically conductive tracer in the various domains, simulation of a conservative, electrically conductive tracer injection was completed. As a baseline for comparison, deviation is compared to modeled electrical results for the entire system spun-up to a uniform, steady-state background concentration of 1000 mg/L. A solute injection was modeled as a constant rate injection at the upstream end of the model domain, where stream concentration was increased from 1000 to 4000 mg/L for a 3-hour constant rate injection. Density affects due to the increased solute concentration were assumed negligible. A total simulation of one week was completed to capture the response of the tracer slowly flushing from the subsurface domain. Model data were extracted at 60 s intervals for the first 24 h of simulation time to resolve rapid changes in concentration through time, and at 360 s intervals for the remaining 144 h of the simulation.

ER modeling used the Conductive DC Media package in COMSOL. The electrical model was used to simulate the injection of direct current and measurement of voltage at the electrodes. A 10-m domain was added beyond the flow and solute transport model domains in all direction to avoid boundary effects in the electrical field (Fig. 1). This added domain remained at initial (background) levels of tracer concentration throughout the simulation. It was added to decrease boundary effects on the electrical model, but assumed to remain at a static concentration to maintain reasonable computational efficiency for the flow and solute transport models. Electrodes were modeled as points located 0.1 m below the model surface, distributed across the model domain (Fig. 2A). Points were located below the surface to represent the shallow penetration achieved by a typical surface array, where electrodes are in contact with the ground at shallow subsurface depths. Quadripole data (i.e., measurements including 4 electrodes as a single potential pair and single current pair) were collected using a modified Schlumberger array (i.e., current driven from outer-most

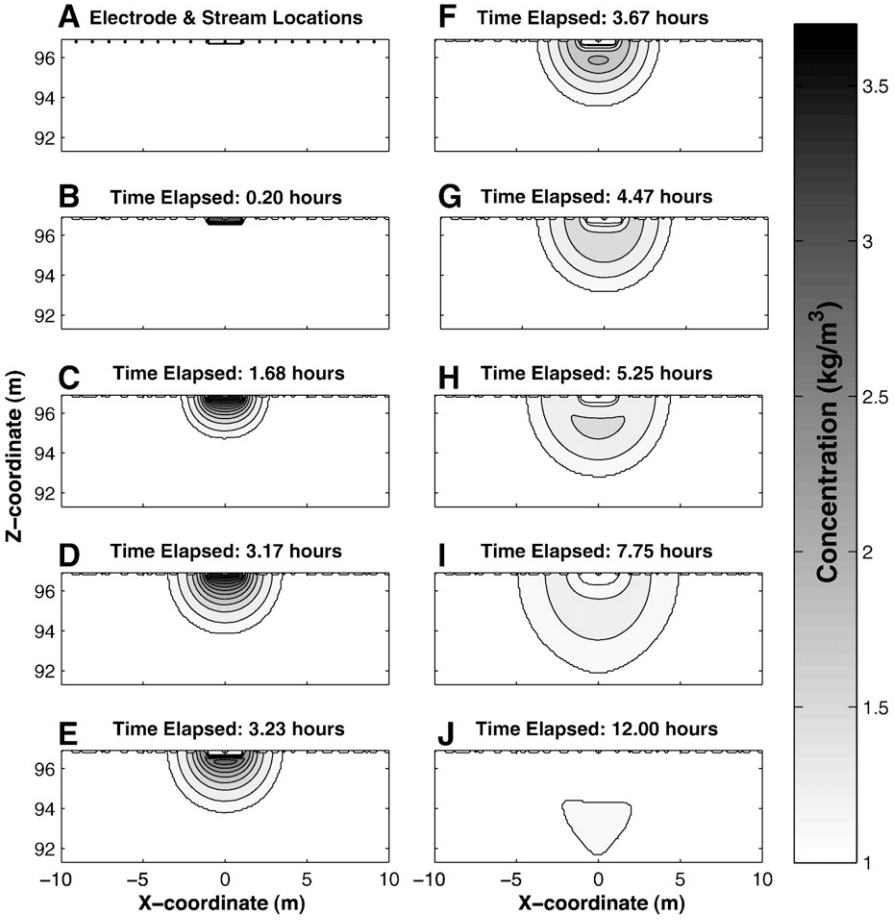

Fig. 2. (A) Stream and electrode locations within model domain. Tracer concentration at background levels (1000 mg/L, uniform) is also shown. (B) Arrival of the tracer is first seen in the stream. (C–D) Diffusion of the tracer into the subsurface, and advection in the hyporheic zone below the stream expand the pulse of tracer in the subsurface. (E–F) Tracer flushes from the stream, leaving a large tracer pulse in the hyporheic zone. (G) A second pulse of tracer appears in the hyporheic zone, transported from temporary hyporheic storage in an upstream pool–riffle-step sequence. (H–J) The advection-dominated hyporheic zone flushes of tracer, leaving a "ring" of tracer in areas dominated by diffusive and rate-limited mass transfer processes.

electrodes, but potential pair not necessarily centered or symmetric within the potential pair). Electrodes were located at $X=0$ (the stream centerline), and $X=\pm 1.1,\ \pm 2.1,\ldots,\pm 11.1$ m (floodplain on either side of the stream). Current was driven from electrodes at $X=\pm 11.1$ m for all measurements. All possible potential pairs were collected. Modeling the electrodes as line or three-dimensional sources from the ground surface to the penetration depth was not attempted because it would have increased computational demand. Because the model's top surface was a no-flux boundary, we felt that placement at this shallow depth would provide more representative current and potential readings, independent of the concentration at the no-flux boundary.

3. Theory

3.1. Electrical resistivity and tracer concentration

Bulk electrical conductivity for the soil–water matrix of a single subsurface domain was calculated using Archie's law [38]. Application of Archie's Law includes the underlying assumptions that there is little to no clay present, and that surface conductivity is substantially less than conductivity through the fluid. Both assumptions are valid for the simulation we completed. For the model domain remaining at background concentration, Archie's Law is applied as:

$$\sigma_b = a\sigma_f\theta^q \tag{3}$$

where σ_b is bulk electrical conductivity [S/m], σ_f is fluid conductivity [S/m], θ is total porosity [unitless], a is a fitting parameter related to tortuosity [unitless], and q is a fitting parameter related to cementation of the matrix [unitless]. Values of $a=1$ and $q=1.3$ are used as representative values to parameterize the finite-element cells, within the ranges commonly accepted in the literature [39]. Bulk apparent electrical conductivity in the porous media is calculated using a bicontinuum formulation of Archie's law (Eq. (4)), [21,40], which incorporates both the MSS and ISS domains:

$$\sigma_b = a(\theta_{MSS}+\theta_{ISS})^{q-1}(\theta_{MSS}\sigma_{MSS}+\theta_{ISS}\sigma_{ISS}) \tag{4}$$

where θ_{MSS} and θ_{ISS} represent the mobile and immobile porosities [–], and σ_{MSS} and σ_{ISS} the mobile and immobile electrical conductivities [S/m].

3.2. Interpretation of electrical measurements

To assess sensitivity of the measurements to the geometry of the ER measurements, 342 quadripoles were simulated. Electrical geophysical methods rely upon Ohm's Law ($R=V/I$) to calculate the electrical resistance of the subsurface, where V is the potential difference measured across the potential pair [V], I is the current driven through a circuit [A], and R is the resistance of the circuit [Ω]. A geometric factor, K [m], is applied to convert between resistance (a property dependent upon the geometry of the electrodes used in a particular measurement) to resistivity (an intrinsic property, the reciprocal of electrical conductivity, which is independent of measurement geometry).

Assuming a homogeneous half-space, the geometric factor can be calculated as:

$$K = \frac{4\pi}{\frac{1}{\overline{AM}} + \frac{1}{\overline{AM_{image}}} - \frac{1}{\overline{AN}} - \frac{1}{\overline{AN_{image}}} - \frac{1}{\overline{BM}} - \frac{1}{\overline{BM_{image}}} + \frac{1}{\overline{BN}} + \frac{1}{\overline{BN_{image}}}} \quad (5)$$

where A and B represent the current pair, M and N the potential pair, and AM, AN, BM, and BN are the distances between electrode pairs. The geometric factor is used with Ohm's Law to calculate apparent resistivity (ρ), [Ωm] as $\rho = KR$. To work in more familiar units of conductivity (which is directly proportional to solute concentration), we convert apparent resistivity to apparent conductivity (σ), where $\sigma = 1/\rho$.

Using the known quadripole geometry and electrical current, a bulk apparent electrical conductivity was calculated for each measurement through time using the Ohm's Law and a formulation of Archie's Law (see the final two paragraphs of Section 3.3). Results were converted from bulk apparent electrical conductivity to percent change from background apparent conductivity (σ_{pc}) to accentuate changes in the electrical signal as follows:

$$\sigma_{pc} = \frac{\sigma(t) - \sigma(t=0)}{\sigma(t=0)}. \quad (6)$$

Fluid concentration was converted to electrical conductivity using the relationship of 2 mg/L = 1 μS/cm [39].

3.3. Temporal moment analysis

The temporal patterns observed inform interpretation of the dominant transport processes. Temporal moments have been used to describe characteristics of solute breakthrough curves including mass arrival, mean arrival time, variance, skewness, and kurtotis of concentration observations through time [41,42]. Temporal moments have been used to drive routing models for streams with transient storage [43], characterize mixing and dilution processes [41,44], and predict solute transport parameters related to RLMT [33,45]. For the remainder of this paper, superscripts "ST" and "ER" are used to denote properties derived from solute transport and electrical resistivity data, respectively.

To highlight the temporal trends in the breakthrough curves observed in both solute transport and ER data we consider analysis of the temporal moments of each data set. An nth order temporal moment (M_n) is calculated by:

$$M_n = \int_0^\infty t^n c(t) dt \quad (7)$$

where t is time, n is the order of the central moment, and $c(t)$ is fluid concentration as a function of time [kg/m^3]. In subsequent equations, M_0 refers to the zeroth temporal moment, M_1 to the first temporal moment, etc. Here, we consider the zeroth through fourth moments, because they are readily interpreted as descriptions of the physical breakthrough curves observed and predicted. Physically, the zeroth moment may be interpreted as the total tracer mass having passed by an observation point, after subtracting the background concentration, normalized by discharge. The first moment, normalized to total mass, is physically interpreted as the mean arrival time of the injected solute at the observation point, calculated as:

$$\mu_1 = \bar{t} = \frac{M_1}{M_0}. \quad (8)$$

The variance of the pulse describes the spread of the breakthrough curve, which may be due to differences in advective flowpaths, as well as diffusive and RLMT processes. Variance is related to the second and lower temporal moments, and is calculated by the following equation:

$$\mu_2 = \sigma^2 = \frac{M_2}{M_0} - \left(\frac{M_1}{M_0}\right)^2. \quad (9)$$

The skewness of the distribution describes the asymmetry of the breakthrough curve; in solute transport studies we expect a positive skewness to result from both diffusive and RLMT processes. A more positive skewness indicates an observed breakthrough curve with a larger degree of tailing behavior. Skewness is related to the third and lower temporal moments, and is calculated by:

$$\mu_3 = \frac{M_3}{M_0} - 3\mu_2 \frac{M_1}{M_0} - \left(\frac{M_1}{M_0}\right)^3. \quad (10)$$

The kurtosis describes the "peakedness" of the distribution. High values indicate a distribution with higher central peaks and fewer extreme events. Kurtosis is related to the fourth and lower temporal moments, and is calculated by:

$$\mu_4 = \frac{M_4}{M_0} - 4\mu_3 \frac{M_1}{M_0} - 6\mu_2 \left(\frac{M_1}{M_0}\right)^2 - \left(\frac{M_1}{M_0}\right)^4. \quad (11)$$

The same temporal moment equation and relevant parameters can be applied to ER data, using Archie's law to convert from apparent electrical conductivity to fluid conductivity. This empirical relationship is applied at initial conditions to establish a tortuosity fitting factor (a) for each quadripole. The forward model was run with $a = 1$ within each finite element. Because measurements are now at a substantially larger scale, it is appropriate to calculate a new fitting factor. Variability in Archie's law parameters across spatial and temporal resolution of measurements may yield misleading estimates of solute concentration [46]. Here, we use observations during pre-injection conditions ($t = 0$ s) to calculate a fitting factor, a, that is appropriate for the spatial scale of each measurement and which yields agreement between known fluid concentration and bulk apparent electrical conductivity. We calculate an effective a for each quadripole (rather than use the value $a = 1$ that parameterized the finite-element model) to enforce agreement between the ER and solute transport models at the initial conditions. At $t = 0$ s, MSS and ISS concentrations are assumed equal. Assuming constant porosity and cementation exponents, a is calculated for each quadripole as:

$$a = \frac{\sigma_{bulk}(t=0)}{\sigma_{fluid}(t=0)\theta^q}. \quad (12)$$

Given apparent bulk conductivity, fluid conductivity in the MSS and ISS domains can be predicted if the distribution of tracer within the MSS and ISS domains is known. In practice the MSS concentration is measured using shallow monitoring wells. The ISS concentration, however, cannot be measured using existing field techniques. Thus, we interpret the data using two cases that define end-members for solute transport. We define Case 1 as the end-member where ISS concentration is equal to MSS concentration (effectively assuming $\alpha = \infty$, or $\theta_{ISS} = 0$). Eq. (3) is applied to solve for fluid conductivity (σ_{MSS}) at each time step for Case 1. We define Case 2 as the end-member where no tracer enters the ISS domain (effectively assuming $\alpha = 0$, thus $\sigma_{ISS} = \sigma_{Background}$). Eq. (4) is used to solve for fluid conductivity (σ_{MSS}) at each time step for Case 2. The case where there is tracer only in the ISS domain is not considered given the short temporal scale of the typical stream-tracer study. The case where more concentration is in the ISS domain would only occur for experiments with very low RLMT exchange coefficients, which would allow the ISS to fill with tracer during a very long tracer injection, and the solute in that domain would then be slowly transferred back to the

MSS domain at timescales much greater than advective flushing of the MSS domain.

To effectively test the ability of ER data to predict solute transport, zeroth through fourth order temporal moments and the associated physical characteristics were calculated for both solute transport and ER simulations. For solute data, moments were based on mobile-domain observations on a 10 cm grid for the stream and subsurface domain at the geophysical transect. For ER data, bulk electrical conductivity at all potential pairs for the geophysical transect was used to calculate temporal moments.

4. Results and discussion

4.1. Flow model

Spatial patterns of hyporheic exchange driven by in-stream geomorphologic features produce the characteristic upwelling and downwelling expected from the streambed profile. Results generally match the two-dimensional patterns published by Gooseff et al. [37]. Velocity along the stream centerline (Fig. 1A) exhibits downwelling and upwelling due to variations in hydrostatic pressure at the streambed.

4.2. Solute transport model

Time-lapse images of solute concentration in the subsurface (Fig. 2) suggest that different transport processes control different regions of the subsurface domain. Advection dominates in the stream and very near-stream subsurface, as tracer is rapidly transported into and out of this region. Beyond this advection-dominated region, however, we observe the effects of RLMT and diffusion controlling solute behavior.

Moving outward from the stream, a region exists in which advective flowpaths flush the tracer from the region below the stream within 5 h of the injection ending (Fig. 2I). Beyond this region of the subsurface, solute exhibits a longer residence time suggesting that RLMT has stored a portion of the tracer temporarily. Continuing outward, a "ring" of tracer has diffused into the hyporheic zone and exchanged with immobile domains. Even when the portion of the hyporheic zone below the stream has returned to background or undetectably low concentrations of tracer, a substantial, distributed mass of tracer continues to diffuse (Fig. 2H–I). As the near-stream subsurface concentration is flushed to lower levels than the diffusive "ring", propagation of the ring into the floodplain stops. Diffusion in both directions continues to control behavior in the subsurface, and tracer is slowly advected down gradient at very low concentrations.

4.3. Process-based signatures in the ER and solute models

Visual inspection of both the solute transport and ER data through time identified four distinct temporal "signatures" collected (representative signatures in Fig. 3, distribution of signatures in Fig. 4A). These signatures describe the shape of the breakthrough curve, and are indicative of solute transport processes at a given location. The four signatures identified are present in both the ER and solute transport data, and may be classified as:

4.3.1. Background signature

Background signatures are those produced by quadripoles exhibiting minimal response to the tracer. The identifying characteristic of background signatures is their lack of response to the tracer. In this study, a threshold of less than 5% change in electrical conductivity was used to classify background signatures. For field data sets, this threshold should be adjusted to identify signatures that are bounded by the noise in the data set. Background signatures were generally located where potential electrode spacing was greater than 9 m. This is expected based on the solute transport model; these measurements are averaging over very large support volumes that are largely dominated by elements where the tracer is not present. For potential pair spacing less than 9 m, background signatures existed for measurements with larger spatial distances between the stream and potential electrodes (Fig. 5).

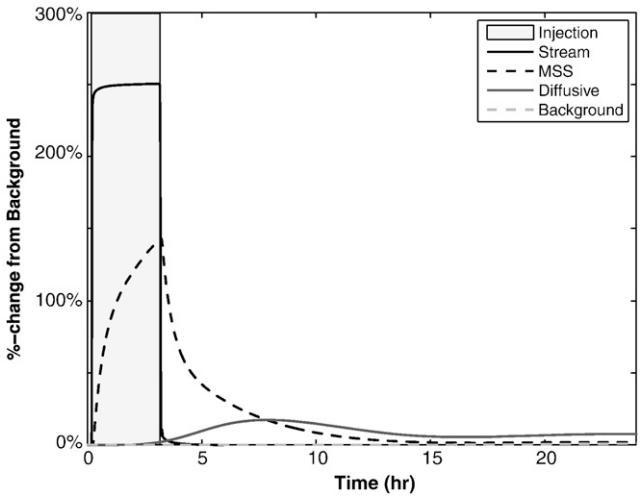

Fig. 3. Representative breakthrough curves for the four identified signatures. The curves shown are representative of the characteristic temporal signatures identified as (1) stream signatures (flat plateau during injection), (2) mobile subsurface signatures (positive correlation to solute transport observations at 50 cm below the streambed), (3) diffusive signatures (negative correlation with solute transport observations at 50 cm below the streambed), and (4) background signatures(overall change of less than 5%). Data plotted are from the solute transport model, though the same signature types are also identified in electrical resistivity data.

4.3.2. Stream signature

The characteristic stream signature is a response that is highly correlated to the simulated in-stream breakthrough curve. Specifically, the stream signature exhibits a rapid response to in-stream conductivity and zero or near-zero gradient during the in-stream plateau. We characterized stream signatures based on the observed data, and not on the physical location of the measurement. Stream signatures generally exist for electrode pairs located very close to the stream with small potential pair spacing (Fig. 5).

4.3.3. Mobile subsurface (MSS) signature

The mobile subsurface signature is identified by a positive correlation with MSS concentration observed at 50 cm below the streambed, at the stream centerline (typical placement for a monitoring well in field studies). The signal responds to the presence of tracer in advective subsurface flow paths by rising initially, and falls when the advective flowpath being sampled is flushed by unlabeled stream water. MSS signatures generally exist for potential pairs centered within 3 m of the stream, and across a range of potential pair spacing (Fig. 5).

4.3.4. Diffusive signature

Interpretation of ER data identified a fourth characteristic signature, identified as a diffusive signature. The diffusive signature response to the spatially distributed, low concentration tracer that remains after flowpaths dominated by advection have been flushed of the tracer. The diffusive flowpath exhibits peak concentration substantially later in time than the stream or mobile subsurface signature. Diffusive signatures respond to the tracer mass that has been transported away from more advective, near-stream flowpaths and is primarily transported by diffusion, both laterally and vertically, away from the stream. Diffusive signatures generally exist for potential pairs with small

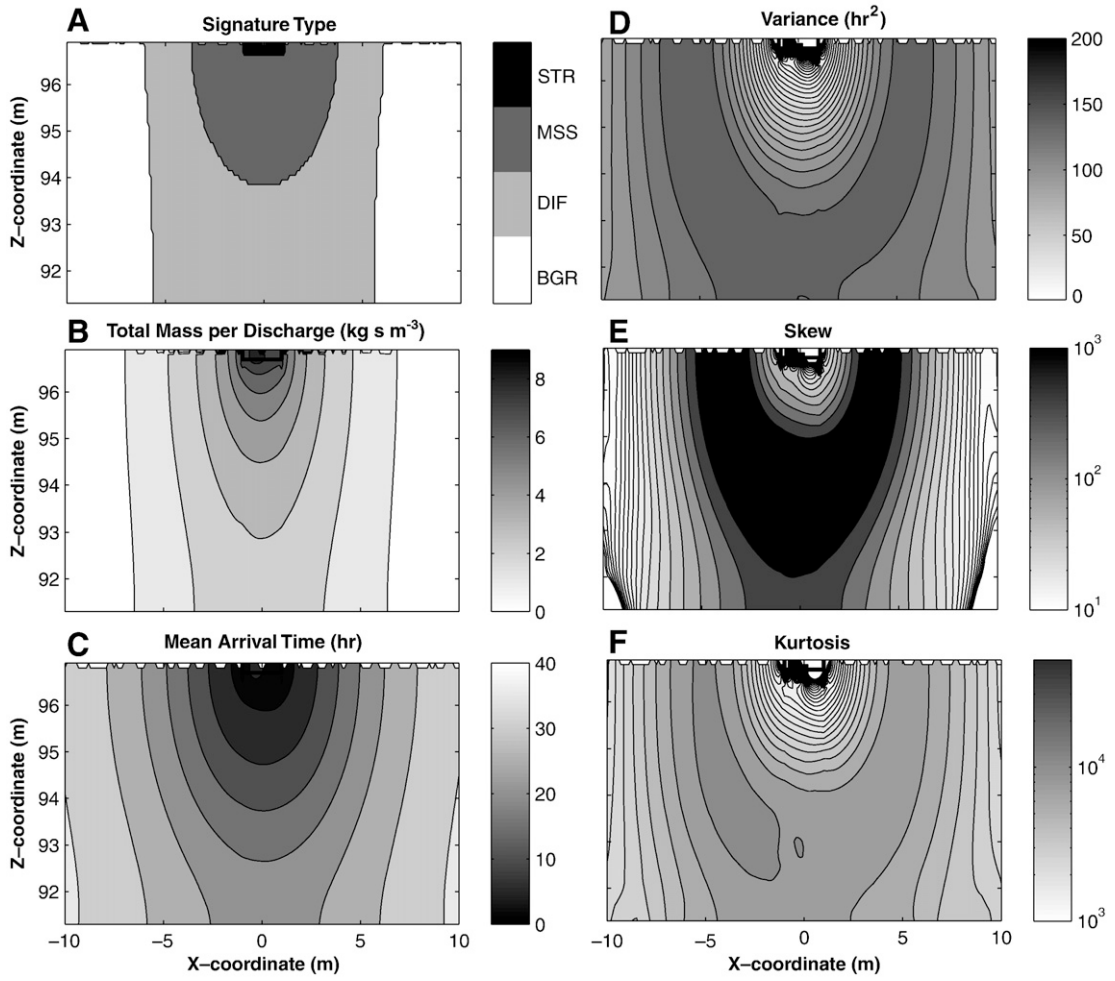

Fig. 4. (A) Spatial distribution of signatures and (B–F) temporal moment interpretations for solute transport in the MSS domain, based on the solute transport simulation. The advection-dominated hyporheic zone below the streambed exhibits similar behavior to the stream itself based on moment analysis of solute data. Outside of this highly advective zone, diffusion and rate-limited mass transfer slow the movement of tracer, yielding a "ring" of highly skewed measurements with substantial tailing behavior. (A) Signature type exhibits a pattern similar to variance and skew, suggesting that diffusive and rate-limited mass transfer processes are dominant in these regions. (B) Total mass normalized by discharge is greatest near the stream and in the advection-dominated region of the hyporheic zone. (C) Average arrival time increases away from the stream. Note the rapid arrival time in the highly advective portion of the hyporheic zone, located below the stream bed. (D) Variance is greatest in a "ring" in the subsurface, which is generally bounded on the interior by the highly advective hyporheic zone. (E) The largest values of skew occur where the primary transport mechanism transitions from advection of diffusion and rate-limited mass transfer. (F) Kurtosis exhibits a similar trend as skew, suggesting that the higher values in the "ring" are due to a more distributed, tailed distribution. Lower kurtosis values indicate a distribution with a more flat plateau near the mean.

spacing, located physically outside of the MSS signature observations (Fig. 5).

Representative signature types for simulated solute transport are readily calculated for the entire subsurface domain (Fig. 4A), and lend to interpretation of solute transport results. We interpret the area defined by the MSS signature as the region typically characterized as the hyporheic zone. Beyond this MSS signature, RLMT slows the movement of the tracer down gradient. This process is not noted in many field studies due to (1) lack of detection ability (i.e., extremely low concentrations are not detectable with field instruments), (2) lack of sufficient monitoring points to characterize this region, (3) time limitations to intensively monitor subsurface wells, and (4) difficulty partitioning RLMT from substrate heterogeneity.

4.4. Spatial trends of solute transport model

Spatial distribution of temporal moments based on solute transport data is explored to understand the rates of tracer movement in the subsurface, and controlling processes in each location (Fig. 4A). Trends in total mass normalized by discharge are as expected (Fig. 4B), with the largest mass passing through the stream channel itself. The darker area of the plot below the stream channel is due to advection of tracer from the stream into the subsurface. Total mass decreases moving away from this highly advective zone (stream and MSS signatures) due to diffusion of the tracer. Mean arrival time (μ_1^{ST}) is highest near the stream and decreases away from the stream (Fig. 4C).

For solute transport data, increased distance from the stream decreases total mass normalized by discharge (Fig. 4B), delays mean arrival time (Fig. 4C), and increases variance (μ_2^{ST}) (Fig. 4D). MSS signatures are spatially aligned with the areas of the largest skew (μ_3^{ST}), suggesting that these signals are most affected by RLMT and diffusion in the subsurface. Stream signatures exhibit a low skew, suggesting that advection overwhelms diffusive and exchange processes that might lead to tailing behavior. Diffusive signatures exhibit a low skew, as they are largely symmetric because their controlling process of diffusion leads to a nearly symmetric breakthrough curve.

Mean arrival time (Fig. 4C) exhibits similar trends to total mass, with mean arrival time in the stream and advective subsurface occurring rapidly. Moving away from the stream, the center of mass arrival is delayed due to the slower diffusive processes transporting tracer into the subsurface. Delayed arrival in the subsurface may also be explained by RLMT slowing the movement of tracer as it diffuses away from the

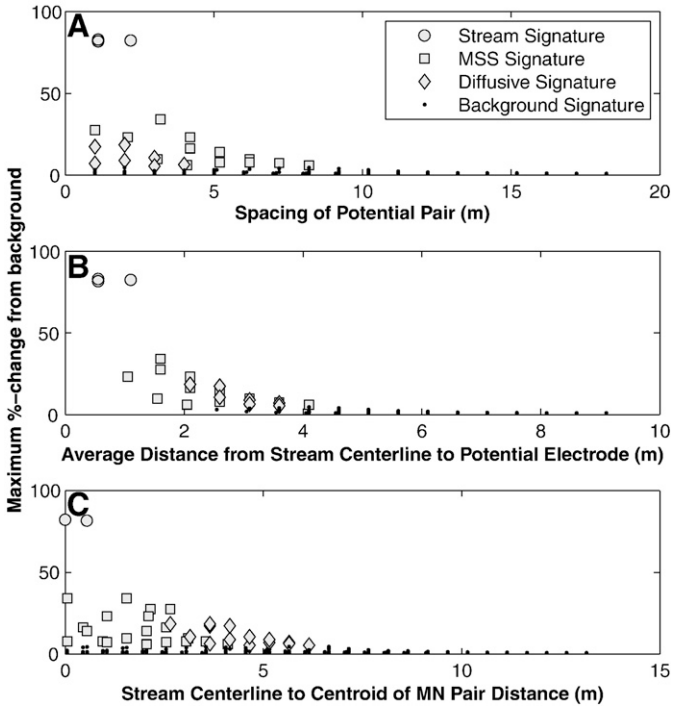

Fig. 5. Spatial trends in the response of quadripoles to the stream solute tracer. The largest responses were stream signatures, located with potential pairs tightly spaced near the stream. Increasing spacing and distance from the stream centerline yields mobile subsurface and diffusive signatures, trending away from the stream centerline. The largest response of electrical resistivity to solute presence is for quadripoles with (A) closely spaced potential pairs, (B) potential electrodes located near the stream, and (C) potential pairs centered on the stream.

stream. Increasing variance in the breakthrough curve farther from the stream suggests that diffusive processes are dominating in these regions of the hyporheic zone. The highly advective stream and subsurface locations exhibit the lowest variance, because advection moves a majority of the tracer through these areas with little diffusive or RLMT influence.

Skewness of the solute transport is an indicator of the relative controls of advection vs. diffusion and transient storage. Transport with only advection and dispersion would exhibit a distribution with minor skew (data are slightly non-gaussian due to diffusion opposing advection for some particles). By including diffusive and RLMT processes, greater positive skew is expected in the data set. Skewness (Fig. 4D) is highly correlated with late-time solute behavior (Fig. 2H–I). The same "ring" pattern exists, suggesting that diffusion into the subsurface and RLMT, which slows the movement of tracer past the transect, is responsible for the tailing behavior observed in the MSS and diffusive signatures.

Physically, we can interpret higher kurtosis (μ_4^{ST}) as an indicator of a single peak of tracer in a given cell. Lower kurtosis values inside the "ring" of higher values (Fig. 4F) suggest that the variance in the observation is controlled by either multiple peaks or more heavily tailed observations. From a physical-process standpoint, we expect that as tracer moves downstream in our pool–riffle sequence that pulses of tracer will leave the highly advective domain and return at later times. The low kurtosis of the near-stream aquifer indicates that the region receives a relatively more varied loading than the surrounding, higher kurtosis region.

4.5. Spatial trends of ER model

Analysis of ER response to the tracer (Fig. 5, presented as maximum percent change from background levels) suggests that maximum electrical response is found for quadripoles that include (1) a more closely spaced potential pair (Fig. 5A), (2) a closer proximity of electrodes to the stream (Fig. 5B), and (3) a measurement that is centered on the stream (Fig. 5C). Also, analysis of maximum response by signature reveals that stream signatures are generally observed from quadripoles with small potential pair spacing near the stream. MSS signatures are present for potential pairs still centered near the stream, but with larger spacing, and diffusive signatures are found for quadripoles with still larger potential pair spacing, and located farther from the stream.

The spatial trends in ER signatures are indicative of the processes that dominate solute behavior within the domain. Based on the simulation completed, we interpret the controlling processes for each signature. Stream signatures indicate quadripoles are sensitive not only to in-stream processes, but rapid diffusion of solute from the stream into the near-stream. The mobile subsurface signature characterizes small spatial and temporal scale advective flowpaths (typically flowpaths within 2.5 m of the stream with mean arrival times less than 8 h). Correlation with simulated MSS data suggests that these quadripoles respond mostly to advection of tracer along short subsurface flowpaths. Diffusive signatures identify a mass transport process that is dominated by diffusion away from the shorter spatial and temporal scale advective flowpath near the stream.

Temporal moments of ER data, for both Case 1 and Case 2, display spatial trends due to the distribution of tracer in the subsurface (Fig. 6, scatter plot). With increasing distance from the stream, total mass normalized by discharge (μ_0^{ER}) decreases, while average arrival time (μ_1^{ER}) and variance (μ_2^{ER}) increase. Skewness (μ_3^{ER}) and kurtosis (μ_4^{ER}) exhibit trends that peak near 3 m and 5 m from the stream, respectively. These results are expected, as the tracer diffuses slowly away from the stream and highly advective hyporheic flowpaths. Spacing of the potential electrodes directly influences the observation, with closer spacing generally resulting in increased total mass, earlier average arrival times, lower variance, higher skew, and lower kurtosis.

The zeroth temporal moment (total mass normalized by discharge) predicted by both Case 1 and Case 2 were substantially lower than the mass flux from the solute transport model (Fig. 6A, F). Case 2 ($ISS = \sigma_{Background}$) was more representative for this model, given the low exchange coefficient defined. This is not necessarily the case for all parameter sets; the analysis using both end-members provides insight regarding the behavior of the system. If Case 1 provides a better fit to field observations, a more rapid exchange between MSS and ISS can be inferred.

4.6. Comparison of ER and solute transport models

Temporal moments based on ER data exhibit reasonable approximations of temporal moments based on solute transport models (Fig. 6). The interpretations of Case 1 and Case 2 differ in their prediction of total solute mass (Fig. 6A, F), but the properties of the distribution based on higher-order temporal moments are identical. This is expected, given that these quantities are all normalized by the zeroth temporal moment. In addition to agreement of general trends, numerical results are reasonably close between solute transport and ER-derived temporal moments, especially for mean arrival time (μ_1) and variance (μ_2). ER measurements integrate across a three-dimensional support volume in the subsurface, which is itself a function of time as electrically conductive solute moves through the subsurface. While true assignment of the measurement to a single point in space and time is not physically possible, we explore patterns in temporal moments by assigning the data a location at the spatial center of potential pair and comparing ER predictions to values derived from vertically averaged solute transport data. Both ER and solute transport results exhibit decreasing total mass, increasing mean arrival time, and increasing variance as observations move spatially farther away from the stream centerline. ER and solute derived parameters exhibit similar patterns in skew and kurtosis, which are similar to the "ring" pattern of tracer observed in the solute transport time lapse images (Fig. 2), in that a local maximum exists with lesser values laterally in either direction. Skew and kurtosis peak at

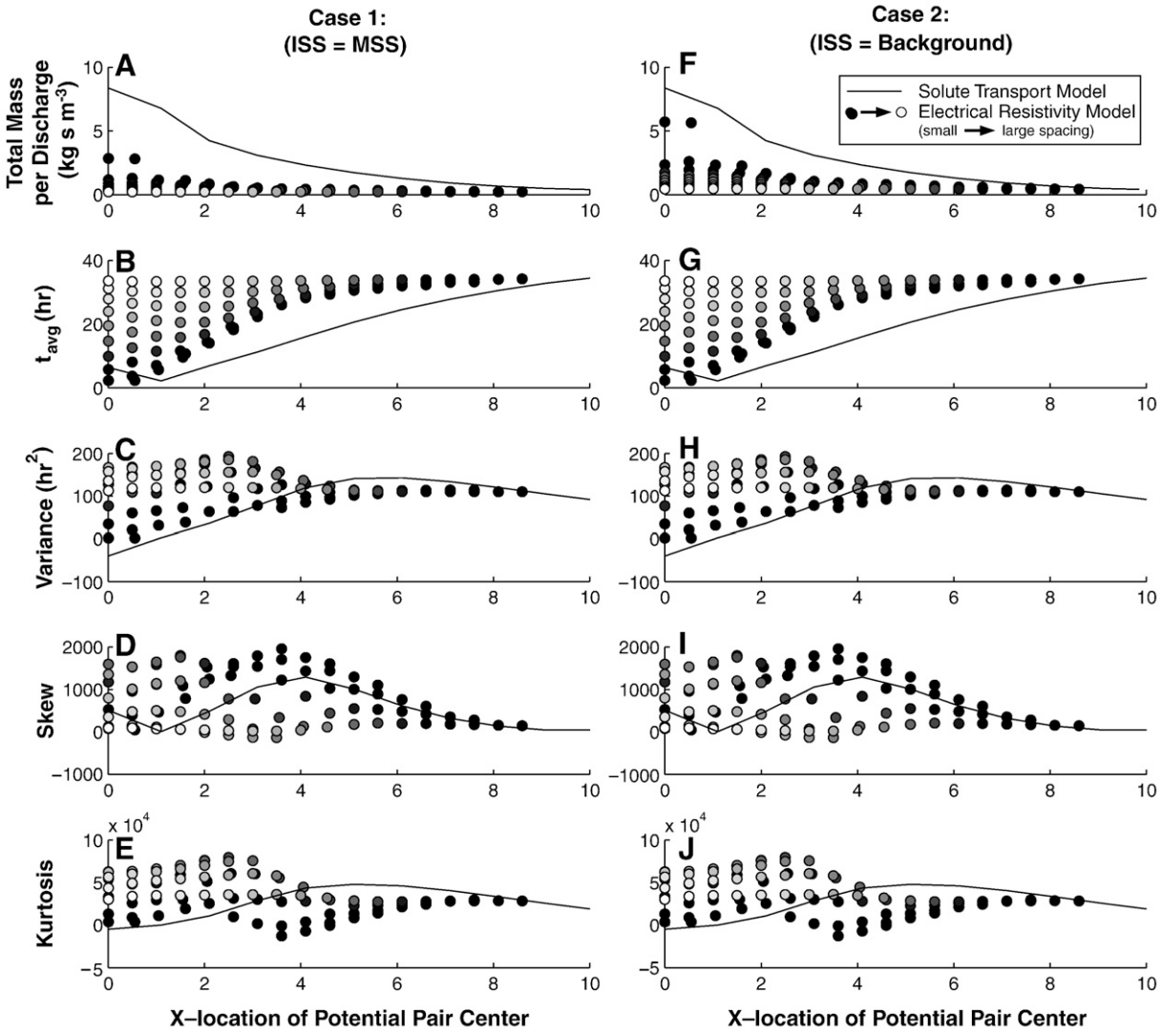

Fig. 6. Spatial trends in temporal moments for both electrical resistivity (ER) data (points) and solute transport (line, vertical average). Point shading represents the spacing of the potential pair (current pair was fixed at ± 11.1 m). Darker points indicate electrodes that are closer to one another. A minimum spacing of 1.0 m and maximum of 18.2 m are represented on the plot as the darkest and lightest points, respectively. ER data are assigned a point in space at the center of the potential pair. We note that assigning apparent resistivity data, which is based on a volumetric measure, to a single point is a flawed assumption, but one commonly used within the electrical geophysics community to explore spatial patterns in uninverted data. Because the model is symmetric, only one side of the floodplain is shown for ease of interpretation. The ability to compare the spatial location of moment data provides insight regarding the locations at which ER can be used to accurately estimate temporal moments of solute transport. Cases 1 and 2 represent end-members of tracer distributions between the MSS and ISS domains. (A and F) Total mass normalized by discharge is under predicted by ER across the entire domain, with the largest error near the stream. (B and G) ER accurately bounds mean arrival time near the stream within a wide range, and generally predicted later arrival time than observed farther from the stream. More closely spaced potential pairs over-predict solute arrival; pairs with greater spacing over-predict mean arrival time. (C and H) Observed variance is bounded by the ER calculated variance. (D and I) Skew of the observed solute transport data is generally well-predicted by ER across the entire domain. Both solute transport and ER moment analysis predict a peak in skew, identifying the location where the propagation of the maximum concentration of solute into the subsurface stops due to flushing of the highly advective hyporheic zone below the stream. (E and J) Kurtosis based on solute transport data is well-predicted by the upper-values of ER calculated kurtosis, and more accurately predicted by quadripoles with larger spacing between the potential pair of electrodes.

approximately 3 m and 4 m from the channel, respectively. The alignment of these thresholds with the general solute transport patterns (Fig. 2) and representative signature plot (Fig. 4A) suggest that ER holds the potential to accurately identify spatial locations where transitions between advection- and diffusion dominated subsurface regions.

Temporal moments based on ER exhibit smaller zeroth moments (μ_0^{ER}, Fig. 6A, F), later mean arrival times (μ_1^{ER}, Fig. 6B, G), and relatively similar variance (μ_2^{ER}, Fig. 6C, H), skew (μ_3^{ER}, Fig. 6D, I), and kurtosis (μ_4^{ER}, Fig. 6E, J) than MSS-derived moments. The larger zeroth moments from direct observation can be explained by the spatial averaging of ER data, since electrical current flows through subsurface domains of varying concentration and always provides some degree of spatial averaging, yielding apparent petrophysical properties which may vary from small-scale, true values [47]. Smaller first moments in ER data compared to solute transport data (Fig. 6B and G, as variance) are likely due to the three-dimensional nature of electrical current paths. Electrical signals travel out of the transverse plane upstream and downstream. Thus, the electrical signal responds to the tracer more quickly than point measurements of MSS concentration.

4.7. Prospects and limitations

The use of ER to provide spatially distributed observations with good temporal resolution is an exciting prospect for hyporheic studies. ER data holds the potential to overcome the “window of detection” issues commonly associated with stream-tracer studies. The ability to track distributed, low-concentration tracer across a substantial subsurface domain can more completely capture the range of residence times and flowpaths within a given stream unit than typical stream-tracer experiment and transport modeling approaches.

ER data may be interpreted to assess ISS concentrations and exchange rates in the subsurface, independently of those observed between stream and hyporheic zones. Finally, properly designed ER data collection may be automated to collect large amounts of data with minimal operational effort by the researcher, minimizing the additional burden on scientists during field studies. The predictive ability of ER data, especially for properties related to lower-order moments, suggests the potential for ER to inform solute transport modeling based on moments [43], or to provide distributed estimates of solute transport parameters [45].

With these benefits come limitations. We reiterate here that the support volume for ER measurements is both dynamic and unknown for a single measurement, requiring data inversion (and its associated uncertainty) to assign spatial distributions with improved resolution. While important quantities derived from temporal moments from ER data generally bound the true values from the solute transport model, variability in the data set exists as a function of spatial location and geometric arrangement of the quadripole (Figs. 5 and 6). Interpretation of these data should be completed with these effects in mind, as the proximity of the quadripole to the tracer affects readings. The spatial locations of ER temporal moments are represented as the center coordinate of the potential pair, and compared to the vertical average of moments from the solute transport model (Fig. 6). The proximity of the tracer pulse to the electrodes affects the ability of ER to accurately detect the pulse [46]. Our ability to collect verification data across the range of domains and temporal scales may be limited by sensitivity of monitoring equipment and subsurface access to sample fluid in the MSS. Hydrologic field techniques do not allow direct assessment of the ISS domain, requiring some degree of interpretation for all data. Finally, we note that ER is limited in accuracy of mass assessment for small, highly concentrated targets and is better suited to assessment of lower, distributed tracer presence [46]. ER monitoring does not replace the need for direct observation, but enhances our ability to follow tracer mass beyond spatial and temporal scales that are typically observed.

In planning a stream–hyporheic tracer study, it is important to consider the strengths and weaknesses of different techniques. Direct observation in the stream and streambed (i.e., via wells) is necessary to capture short, rapid flowpaths. Coupling direct observation with an ER array focused on slower, deeper flowpaths and tracking more diffuse mass transport processes in the relatively deeper aquifer and floodplains would compliment the observational data set. By targeting different spatial locations and temporal scales with unique observational methods, a new data stream can be collected to refine solute transport models. ER extends our ability to track mass in space and time, and can account for mass that is otherwise lost during traditional studies.

5. Conclusions

This work has demonstrated that electrical resistivity measurements during stream–hyporheic solute transport experiments provide a distributed data set inclusive of both mobile and immobile subsurface domains. Interpretation of these data allows scientists to parameterize more complex models that include RLMT (i.e., diffusion between domains of varied mobility) in the subsurface, a process that has been identified as important but largely overlooked in stream modeling efforts. Temporal moment analysis has been shown to be a promising tool in interpretation of ER data, and in identification of dominant solute transport processes.

The long-term presence of solute in the subsurface, diffusing laterally and vertically away from the stream and highly advective flowpaths, suggests a potential fate for tracer that is otherwise “lost” from downstream measurements. Our analysis of spatial patterns and ER data identifies four representative signatures (stream, MSS, diffusive, and background), and their spatial distribution in the subsurface. Traditional hyporheic monitoring in-stream and in the streambed is largely focused on stream and MSS signatures, overlooking the larger and slower diffuse signatures. Tracer mass that would otherwise be unaccounted for can be tracked through time and space via minimally invasive ER monitoring. Typical patterns identified here may provide an initial template for planning both ER and direct solute monitoring efforts; observations can be focused in the locations where the method and processes are well matched. For example, direct monitoring of highly advective hyporheic flowpaths with monitoring wells is appropriate, whereas ER provides better data in larger, slower tracer distributions. Thus, ER does not replace the need for traditional in-stream and monitoring well measurements. Rather, ER supplements these data streams by providing a distributed assessment in more slowly changing regions of the subsurface.

Simulation of mass transport by the solute transport model compared to ER-derived quantities demonstrated that estimation of solute concentration by ER is generally lower than directly observed values, yet temporal trends are visually similar. The reduced total mass values are likely because ER is averaging over a spatially complex support volume of heterogeneous concentration, while solute transport observations are point measurements in space and time. In comparison to observed MSS data, ER under predicts fluid concentration, though adequately captures spatial and temporal trends in the model domain.

Numerical simulations of this type can be used to plan for ER monitoring of stream–hyporheic tracer studies at laboratory model (e.g., flume) or field-scale studies. The coupled model allows experimentalists to consider a range of conditions that could be expected in the field. Simulation of several potential ER electrode arrays could help design the most efficient array for the expected tracer transport, and can be used to determine if surface or down-well electrodes would be more logical for researchers' objective for an experiment. Finally, these simulations allow planning of the appropriate level of solute to be released during a tracer study, ensuring that tracer levels are maintained at as low of levels as feasible to minimize environmental impact.

Future work should attempt to identify the same patterns observed here in field data, and correlate ER and solute data in a heterogeneous, unsteady-state setting. The assumptions of a homogeneous, isotropic subsurface are a limitation of this study that should be tested in future work. Differences in hydraulic conductivity and measurement support may also lead to discrepancies between ER and fluid conductivity measurements. Additionally, sensitivity analysis to model parameters (e.g., RLMT coefficient, porosity, etc.) was not completed. Predictions of solute transport parameters would be improved by combining observed ER signals in the field, direct observation in streams and monitoring wells, and a numerical model. A limited number of intensive field or large-scale laboratory studies with comprehensive monitoring would aid in determining more precisely the processes (and their relative speeds) that are well characterized by ER.

Acknowledgements

This material is based upon work supported by the National Science Foundation's Hydrologic Sciences program, under grant no. EAR-0911435. Any opinions, findings, and conclusions or recommendations expressed in this material are those of the authors and do not necessarily reflect the views of the National Science Foundation. We thank three anonymous reviewers for comments that improved the manuscript.

References

[1] Wondzell SM, Swanson FJ. Seasonal and storm dynamics of the hyporheic zone of a 4th-order mountain stream. 1: Hydrologic processes. J North Am Benthological Soc 1996;15:3–19.
[2] Morrice J, Valett H, Dahm C, Campana M. Alluvial characteristics, groundwater–surface water exchange and hydrological retention in headwater streams. Hydrol Process 1997:11.

[3] Boulton AJ, Findlay S, Marmonier P, Stanley EH, Valett HM. The functional significance of the hyporheic zone in streams and rivers. Annu Rev Ecol Syst 1998;29:59–81.
[4] Findlay S. Importance of surface–subsurface exchange in stream ecosystems: the hyporheic zone. Limnol Oceanogr 1995;40:159–64.
[5] Valett H, Morrice J, Dahm C, Campana M. Parent lithology, surface–groundwater exchange, and nitrate retention in headwater streams. Limnol Oceanogr 1996: 333–45.
[6] Haggerty R, Gorelick S. Design of multiple contaminant remediation: sensitivity to rate-limited mass transfer. Water Resour Res 1994;30.
[7] Harvey C, Gorelick S. Rate-limited mass transfer or macrodispersion: which dominates plume evolution at the Macrodispersion Experiment (MADE) site. Water Resour Res 2000;36.
[8] Haggerty R, Wondzell S, Johnson M. Power-law residence time distribution in the hyporheic zone of a 2nd-order mountain stream. Geophys Res Lett 2002;29:1640.
[9] Bencala K, Walters R. Simulation of solute transport in a mountain pool-and-riffle stream: a transient storage model. Water Resour Res 1983;19:718–24.
[10] Goltz M, Roberts P. Three-dimensional solutions for solute transport in an infinite medium with mobile and immobile zones. Water Resour Res 1986;22:1139–48.
[11] Ruehl C, Fisher A, Hatch C, Huertos M, Stemler G, Shennan C. Differential gauging and tracer tests resolve seepage fluxes in a strongly-losing stream. J Hydrol 2006;330:235–48.
[12] Payn R, M Gooseff, B McGlynn, K Bencala, S Wondzell. Channel water balance and exchange with subsurface flow along a mountain headwater stream in Montana, USA. Water Resources Research. (In Press).
[13] Harvey JW, Wagner BJ. Quantifying hydrologic interactions between streams and their subsurface hyporheic zones. In: Jones JB, Mulholland PJ, editors. Streams and Ground Waters; 2000. p. 3–44.
[14] Wagner B, Harvey JW. Experimental design for estimating parameters of rate-limited mass transfer: analysis of stream tracer studies. Water Resour Res 1997;33:1731–41.
[15] Marion A, Zaramella M, Packman A. Parameter estimation of the transient storage model for stream–subsurface exchange. J Environ Eng 2003;129:456–63.
[16] Wondzell S. Effect of morphology and discharge on hyporheic exchange flows in two small streams in the Cascade Mountains of Oregon, USA. Hydrol Process 2006;20:267–87.
[17] Gooseff MN, McKnight DM, Runkel RL, Vaughan BH. Determining long time-scale hyporheic zone flow paths in Antarctic streams. Hydrol Process 2003;17: 1691–710.
[18] Harvey JW, Wagner BJ, Bencala KE. Evaluating the reliability of the stream tracer approach to characterize stream–subsurface water exchange. Water Resour Res 1996;32:2441–51.
[19] Briggs M, Gooseff M, Arp C, Baker MA. A method for estimating surface transient storage parameters for streams with concurrent hyporheic storage. Water Resources Research; 2008.
[20] Acworth R, Dasey G. Mapping of the hyporheic zone around a tidal creek using a combination of borehole logging, borehole electrical tomography and cross-creek electrical imaging, New South Wales, Australia. Hydrogeol J 2003;11:368–77.
[21] Singha K, Day-Lewis F, Lane J. Geoelectrical evidence of bicontinuum transport in groundwater. Geophys Res Lett 2007;34:12401.
[22] Binley A, Henry-Poulter S, Shaw B. Examination of solute transport in an undisturbed soil column using electrical resistance tomography. Water Resour Res 1996;32:763–9.
[23] Slater L, Binley A, Daily W, Johnson R. Cross-hole electrical imaging of a controlled saline tracer injection. J Appl Geophys 2000;44:85–102.
[24] Slater L, Binley A, Versteeg R, Cassiani G, Birken R, Sandberg S. A 3D ERT study of solute transport in a large experimental tank. J Appl Geophys 2002;49:211–29.
[25] Cassiani G, Bruno V, Villa A, Fusi N, Binley A. A saline trace test monitored via time-lapse surface electrical resistivity tomography. J Appl Geophys 2006;59:244–59.
[26] Kemna A, Kulessa B, Vereecken H. Imaging and characterisation of subsurface solute transport using electrical resistivity tomography (ERT) and equivalent transport models. J Hydrol 2002;267:125–46.
[27] Slater L, Binley A, Brown D. Electrical imaging of fractures using ground-water salinity change. Ground Water 1997;35:436–42.
[28] Ward AS, Gooseff MN, Singha K. Imaging hyporheic zone solute transport using electrical resistivity. Hydrol Process 2010;24:948–53.
[29] Crook N, Binley A, Knight R, Robinson D, Zarnetske J, Haggerty R. Electrical resistivity imaging of the architecture of substream sediments. Water Resour Res 2008;44.
[30] Blöschl G, Sivapalan M. Scale issues in hydrological modelling: a review. Hydrol Process 1995;9:251–90.
[31] Vasco D, A Datta-Gupta, J Long. Resolution and uncertainty in hydrologic characterization. Water Resources Research. 33.
[32] Daily W, Ramirez A. Electrical resistance tomography during in-situ trichloroethylene remediation at the Savannah River Site. J Appl Geophys 1995;33:239–49.
[33] Singha K, Pidlisecky A, Day-Lewis F, Gooseff M. Electrical characterization of non-Fickian transport in groundwater and hyporheic systems. Water Resour Res 2008;44.
[34] Day-Lewis F, Singha K, Binley A. Applying petrophysical models to radar travel time and electrical resistivity tomograms: resolution-dependent limitations. J Geophys Res 2005;110:B08206.
[35] Runkel RL. One-dimensional Transport with Inflow and Storage (OTIS): A Solute Transport Model for Streams and Rivers. US Dept. of the Interior, US Geological Survey; Information Services; 1998. distributor.
[36] COMSOL I. 3.5, User's Guide and Reference Guide. Burlington, USA: COMSOL; 2008.
[37] Gooseff MN, Anderson JK, Wondzell SM, LaNier J, Haggerty R. A modelling study of hyporheic exchange pattern and the sequence, size, and spacing of stream bedforms in mountain stream networks, Oregon, USA. Hydrol Process 2006;20:2443–57.
[38] Archie G. The electrical resistivity log as an aid in determining some reservoir characteristics. Am Inst Min Met Eng, Tech Pub 1942;1422.
[39] Keller G, Frischknecht F. Electrical Methods in Geophysical Prospecting. Oxford, UK: Pergamon Press; 1966.
[40] Day-Lewis F, Lane J, Gorelick S. Combined interpretation of radar, hydraulic, and tracer data from a fractured-rock aquifer near Mirror Lake, New Hampshire, USA. Hydrogeol J 2006;14:1–14.
[41] Gupta A, Cvetkovic V. Temporal moment analysis of tracer discharge in streams: combined effect of physicochemical mass transfer and morphology. Water Resour Res 2000;36.
[42] Harvey C, Gorelick S. Temporal moment-generating equations: modeling transport and mass transfer in heterogeneous aquifers. Water Resour Res 1995;31.
[43] Schmid BH. Temporal moments routing in streams and rivers with transient storage. Adv Water Resour 2003;26:1021–7.
[44] Cirpka O, Kitanidis P. Characterization of mixing and dilution in heterogeneous aquifers by means of local temporal moments. Water Resour Res 2000;36:1221–36.
[45] Day-Lewis F, Singha K. Geoelectrical inference of mass transfer parameters using temporal moments. Water Resour Res 2008;44:W05201.
[46] Singha K, Gorelick S. Effects of spatially variable resolution on field-scale estimates of tracer concentration from electrical inversions using Archieís law. Geophysics 2006;71:G83.
[47] Singha K, Gorelick S. Hydrogeophysical tracking of three-dimensional tracer migration: the concept and application of apparent petrophysical relations. Water Resour Res 2006;42:W06422.